Received: 16 May 2023 | Revised: 6 October 2023 | Accepted: 20 November 2023

DOI: 10.1002/jor.25747

Journal of Orthopaedic Research®

RESEARCH ARTICLE

Covariations between scapular shape and bone density in B-glenoids: A statistical shape and density modeling-approach

Nazanin Daneshvarhashjin[1] | Philippe Debeer[1,2] | Bernardo Innocenti[3] | Filip Verhaegen[1,2] | Lennart Scheys[1,2]

[1]Department of Development and Regeneration, Institute for Orthopaedic Research and Training (IORT), Faculty of Medicine, KU Leuven, Leuven, Belgium

[2]Division of Orthopaedics, University Hospitals Leuven, Leuven, Belgium

[3]BEAMS Department (Bio Electro and Mechanical Systems), Université Libre de Bruxelles, Brussel, Belgium

Correspondence
Nazanin Daneshvarhashjin, Department of Development and Regeneration, Institute for Orthopaedic Research and Training (IORT), Faculty of Medicine, KU Leuven, Herestraat 49-bus 7003 68, Leuven 3000, Belgium.
Email: Nazanin.daneshvarhashjin@kuleuven.be

Funding information
Interreg Vlaanderen-Nederland, Grant/Award Number: ZL3C150100-401; Zimmer Biomet, Grant/Award Number: EDW-ZIMMER-O2030

Abstract

B-type glenoids are characterized by posterior humeral head migration and/or bony-erosion-induced glenoid retroversion. Patients with this type of osteoarthritic glenoids are known to be at increased risk of glenoid component loosening after anatomic total shoulder arthroplasty (aTSA). One of the main challenges in B glenoid surgical planning is to find a balance between correcting the bony shape and maintaining the quality of the bone support. This study aims to systematically quantify variabilities in terms of scapular morphology and bone mineral density in patients with B glenoids and to identify patterns of covariation between these two features. Using computed tomography scan images of 62 patients, three-dimensional scapular surface models were constructed. Rigid and nonrigid surface registration of the scapular surfaces, followed by volumetric registration and material mapping, enabled us to develop statistical shape model (SSM) and statistical density model (SDM). Partial least square correlation (PLSC) was used to identify patterns of covariation. The developed SSM and SDM represented 85.9% and 56.6% of variabilities in terms of scapular morphology and bone density, respectively. PLSC identified four modes of covariation, explaining 66.0% of the correlation between these two variations. Covariation of posterior–inferior glenoid erosion with posterior sclerotic bone formation in association with reduction of bone density in the anterior and central part of the glenoid was detected as the primary mode of covariation. Identification of these asymmetrical distribution of bone density can inform us about possible reasons behind glenoid component loosening in B glenoids and surgical guidelines in terms of the compromise between bony shape correction and bone support quality.

KEYWORDS
B glenoids, partial least square correlation, shoulder osteoarthritis, statistical density modeling, statistical shape modeling

1 | INTRODUCTION

Anatomic total shoulder arthroplasty (aTSA) improves joint function and relieves pain in patients with shoulder osteoarthritis (OA).[1–3] However, aTSA is not free from complications.[1–3] One of the most frequent complications is glenoid component loosening, with an increasing prevalence of 1.2% per annum following implantation.[3–6] Especially, osteoarthritic glenoids characterized by posterior humeral head migration and/or bony-erosion-induced glenoid retroversion, that is, B-type glenoids according to the

Filip Verhaegen and Lennart Scheys shared last authorship.

Walch classification, are at increased risk of glenoid component loosening.[2]

Surgical techniques for addressing B glenoids during aTSA vary from high-side reaming for retroversion correction, over concentric reaming without version correction, to the use of augmenting posterior components.[2,7] High-side reaming of the glenoid toward a more neutral version is the most frequently used technique.[2,8] However, its association with bone removal of the anterior, none-roded part of the glenoid further complicates implant survival.[8,9] Indeed, one of the main challenges in B glenoid surgical planning is that shoulder surgeons typically need to compromise between glenoid version correction (bone shape) and quality of bone support.[10] However, the optimal guideline for this compromise thus far remains unknown.[11]

Previous literature emphasized the association between reduced glenoid BMD and elevated risk of glenoid component fixation failure.[12–14] Preservation of the dense subchondral bone of the glenoid has been suggested to be an important factor in providing uniform underlying support for the implant and therefore in decreasing implant failure.[15] Therefore, assessing bone quality in aTSA typically involves detecting regions of high bone density.[16] Past research reported B glenoids to have a nonuniform bone mineral density distribution (BMDD), with posterior quadrants of the glenoid typically being more dense.[15–17] Unfortunately, the BMDD assessment in the glenoid region is mostly limited to average values within large subregions of the glenoid. Therefore, it remains unknown if, and how, these BMDD patterns vary in function of known variations in the scapular shape of B glenoids. A more detailed quantification of BMDD in B glenoids and their possible association with scapular shape variations thus has great potential toward a better-informed planning of aTSA and, in the longer term, the reduction of glenoid component loosening in those challenging cases with B glenoids.

Statistical shape modeling (SSM) and statistical density modeling (SDM) through principal component analysis (PCA) is the current gold standard approach to independently identify dominant variability patterns within a population.[18] Recent studies developed SSM, and SDM for B glenoid and healthy population.[11,19] To generate more authentic and realistic models encompassing both bone shape and density, the association between SSM and SDM was assessed through Pearson correlation analysis, which revealed no strong correlations.[11,19] However, simple correlation coefficients may overlook the existing correlations. The partial least squares correlation (PLSC) method, in turn, can capture complex relationships and reveal hidden patterns of covariations in the data that are not apparent when looking at individual correlations and it can enable the identification of possible covariations between both of these components.[20,21] To the best of our knowledge, this method has not already been applied to B glenoids. The objectives of this study are therefore to: (1) identify modes of variations in terms of scapular morphology and bone mineral density in a representative cohort of patients with B glenoids and (2) explore potential patterns of covariation between these two features.

2 | METHOD

The ethical committee of the University Hospitals Leuven (S58348) approved this retrospective, case-control study (Level III).

2.1 | Study population

Sixty-four patients with shoulder OA and B glenoids, planned for total shoulder arthroplasty at our institution were retrospectively selected from an existing data set.[22] The mean age and body mass index (BMI) of the patients were 65.0 ± 10.6 years and 29.7 ± 6.6 (mean ± standard deviation [SD]), respectively. Patients were 45% male and 55% female, and the investigated shoulders were 43% left and 57% right shoulders. The study population covers all three subtypes of B glenoids based on Bercik et al.[23] classification (B1 = 28, B2 = 22, and B3 = 14). Full scapular computed tomography (CT) images were obtained for the patients with the scan parameters listed in Table 1.

2.2 | SSM

We applied a recently in-house developed SSM approach which has been validated for healthy scapulae.[24] CT scan images were segmented using semi-automatic threshold-based method in Mimics (version 22.0; Materialise®), and three-dimensional (3D) scapular shapes were reconstructed (Figure 1(1-A)).[24] To obtain point-to-point correspondences between scapular shapes, using MeshMonk open-source software,[25] rigid registration was performed between each of the training scapulae and a randomly selected subject chosen as the initial template shape. Subsequently, using a visco-elastic model, the shape of the template was deformed to match the shape of the target scapular surface to perform a nonrigid registration[24,25] (Figure 1(1-B)). These steps were iteratively repeated using the mean shape (μ_S) of the registered subjects from the previous iteration as the template. This approach aimed to remove any possible bias associated with the initially selected template and to find a population-based mean template for registering local glenoid erosions. The resulting template surface mesh was represented by 32,487 nodes and 64,970 triangular (tri) elements. For each training scapula, the vertex coordinates for all nodes (n = K) were expressed as a vector ($X = (x_1, y_2, z_3, \ldots, x_k, y_k, z_k)$), describing the scapular shape. Once correspondences were defined, all scapular surfaces were realigned into a common coordinate system using a generalized Procrustes analysis without scaling.[26] Finally, PCA (MeshMonk[25]) was applied to the concatenated vertex coordinate data of all scapular surfaces in the training data set and the data set was reduced to principal components (PCs). These PCs were then used to develop an SSM of the scapulae, describing the main modes of shape variation. Modes of variation were interpreted by perturbing the μ_S by $\pm 2SD_{SSM}$ which represents the 95% confidence interval (Figure 1(2)).[11,18] Each scapula's PC scores were retained for the assessment of covariation patterns between bone shape and BMDD.

TABLE 1 Scan parameters of the CT images.

Number of patients	Scanner	Pixels	Tube voltage (mean ± SD) (kilovolatge peak)	Slice thickness (mean ± SD) (mm)	Pixel spacing (mean ± SD) (mm)	Reconstruction algorithm
57	Brightspeed	512 × 512	120 ± 0.0	0.67 ± 0.18	0.54 ± 0.02	Bone plus
7	Somatom	512 × 512	108.5 ± 9.9	1.09 ± 0.40	0.48 ± 0.04	Br59, Br59s, and Br 60

Abbreviation: CT, computed tomography.

2.3 | SDM

To develop the SDM, we used the same training data set as the one employed for the SSM. Based on the surface template, created in our SSM, a volumetric template mesh was created in 3-matic (version 15.0; Materialise®). 1464064 four-node linear tetrahedral elements with a mean volume of 0.06 mm^3 were created. As the mean of element edge lengths was on the order of the scan resolution, the elements were sufficient to capture BMDD. This template was then elastically morphed to each subject by displacing the surface nodes of the template toward the corresponding surface nodes of that subject,[11] using a developed in-house Python script in Abaqus 6.14 software (Dassault Systemes Simulia Crop.) (Figure 1(3-A)). As a result of the imposed mesh connectivity, the inner volumetric mesh uniformly deformed accordingly (Figure 1(3-A)). Each volumetric scapular mesh was then transformed back into its original CT coordinates and the average Hounsfield units (HU) within the associated CT image volume were assigned to each volumetric mesh' node, without distinguishing between cortical and cancellous bone (Figure 1(3-B)). To account for potential surface artifacts caused by segmentation, discretization, and partial volume effect in the source CT data, 2 mm of the outer bony surface elements were excluded from our variation analysis by assigning a constant uniform HU value of 900, representing the HU value of the cortical bone. Therefore, these values were not included in the variation analysis due to their constant values in all training data sets. Afterward, PCA was applied to a subregion of the scapula, that is, the region of interest for implant positioning in aTSA (Figure 1(3-B)). To consistently define this region across the data set, nodes were first selected on the template shape on the glenoid side of a plane defined in parallel with the glenoid plane and transecting the spinoglenoid notch (Figure 1(3-B)) and this selection was then applied to the other scapulae based on the available correspondences. For each scapula, the bone densities in HU at all nodes of the region of interest (n = N) were expressed as a vector (HU = (HU_1, HU_2, ..., HU_N)). The vectors of bone densities for all subjects were assembled into a matrix. Finally, SDM was established through PCA, describing the main BMDD variation modes with respect to the mean BMDD (μ_I). Similar to SSM, variation modes were described, and each subject's PC scores were retained (Figure 1(4)). To visualize each mode, the mean volumetric mesh was utilized, and the calculated HU values for each mode were assigned. Color maps representing the HU values were then generated using ParaView (version 4.4.0; Kitware).

2.4 | Evaluation of the models

To evaluate the compactness of both models, the cumulative percentages of the explained variability by all significant modes were calculated.[18,27] Furthermore, the root means square generalization error (RMSE) of SSM and SDM for each specimen was calculated using leave-one-out evaluation.[11,27] The average RMSE was then calculated across all subjects. To remove noise and detect only significant modes of variations in both models, the number of significant PC modes was defined based on the rank of roots algorithm, following 10,000 permutation tests.[28]

2.5 | Covariation between scapular shape and bone quality

To assess covariations between the significant modes of scapular shape and BMDD, the PLSC method was used. This method allows the detection of scapular morphology variations patterns that have the most covariation with BMDD variation patterns. The PLSC method, based on the singular value decomposition of the covariance matrix, can identify shared information between PC scores of SSM and SDM. Hereto, PC scores of SSM and SDM are reduced to smaller new pairs of uncorrelated latent variables while maximizing the covariance between the two data sets.[20,29] This smaller set of uncorrelated components, derived as linear combinations of the original variables (SSM and SDM PC scores), representing each mode of covariation with the first pair accounting for the largest amount of covariation, the second pair for the next largest amount, and so on.[30] The statistical significance of each PLSC mode was tested using 10,000 random permutation tests.[31]

2.6 | Clinical interpretation

To describe the distinctive impact of the first four significant modes of SSM on variations in anatomical scapular shape, we employed two contemporary methodologies: (1) we perturbed the average shape (μ_S) by ±2SD (Figures 1 and 2), thereby generating 3D models of the scapulae corresponding to each SSM mode (Figures 1 and 2). Subsequently, we conducted anatomical measurements on these generated models (μ_S +2SD, and μ_S −2SD) for each mode to define which anatomical variations occur in each mode[32]; (2) we performed 14 anatomical measurements for all training subjects and thereby calculated Pearson correlation coefficients relating these anatomical

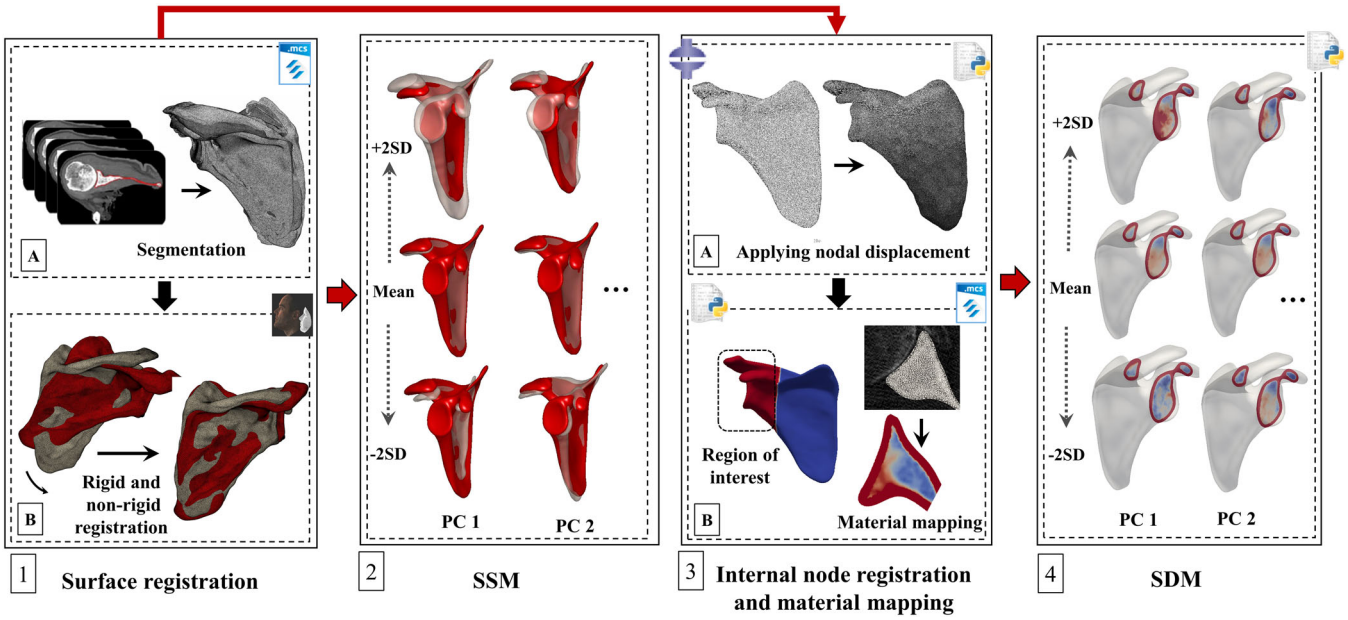

FIGURE 1 Workflow for SSM and SDM: (1-A) Segmenting CT Scan images; (1-B) Rigid and no-rigid surface registration of a scapula (red scapula), using the surface template (white scapula); (2) SSM with PCA; (3-A) Elastically deforming the volumetric template mesh (white scapula) to a random subject by displacing surface nodes (grayscale indicates the magnitude of required displacement for each node of the subject, with darker regions representing greater displacements); (3-B) Material mapping in the region of the interest; and (4) SDM with PCA. CT, computed tomography; PCA, principal component analysis; SDM, statistical density model; SSM, statistical shape model. [Color figure can be viewed at wileyonlinelibrary.com]

measurements and subjects' PC scores.[11] Specifically, the PC scores of each of the modes of variation of all included subjects ($n = 62$) were correlated to each of the 14 anatomical measurements taken for those subjects. The same methodology was used for describing variations in anatomical scapular shape corresponding to each PLSC mode.

The anatomical measurements were acquired using a modified version of a previously published automated algorithm.[22] The modification specifically accounted for defining the scapular plane based on the most important landmarks of the scapular body while avoiding the possibly errored glenoid surface: supraspinatus fossa, the scapular lateral pillar, trigonum spinae region, the inferior angle of the scapula, and the medial border of the scapula.[33,34] The measurements include glenoid version, inclination, height, and width, as well as scapular offset, critical shoulder angle (CSA), posterior acromial slope (PAS), and lateral acromial angle (LAA). The orientation of coracoacromial complex was also defined by measuring coracoid–scapular plane angle, anterior acromion–scapular plane angle, posterior acromial–scapular plane angle, coracoid–posterior acromial angle, fulcrum axis, and fulcrum axis ratio. The anatomical measurements were conducted similarly as described in detail in previous studies of Verhaegen et al.[22,24] To briefly describe the less common measurements in this study, the acromial plane was fitted to the inferior area of the acromion, and the glenoid plane was fitted to the glenoid surface. The LAA was then measured as the angle between the normal vectors of the acromial and glenoid planes, while PAS was measured as an angle between the normal vectors of the acromial and scapular planes.

In addition, we analyzed to what extent modes of covariations were influenced by biometric data (gender [female = 0; male = 1], age, BMI, and shoulder side), by computing Pearson correlation coefficients. Bonferroni adjustments were applied to account for multiple comparisons. This adjustment involved dividing the significance level (0.05) by the total number of tests to have a more stringent statistical significance threshold.[35]

3 | RESULTS

Due to severe glenoid erosions and localized deformations, 2 out of 64 subjects could not undergo surface and volumetric registration. Therefore, the reported findings are based on 62 subjects.

3.1 | Evaluation of the statistical models (SSM and SDM)

The compactness of the SSM and SDM defined the cumulative percentage of explained variability as each PC mode is added (Figure 2A,B [red lines]). The significance test identified 8 and 14 significant uncorrelated and independent PC modes ($p < 0.001$), representing 85.85% (Figure 2A) and 56.59% (Figure 2B) of the training data set variability, respectively. The average RMSE associated with each number of PC modes for the SSM and SDM based on the leave-one-out evaluations are shown in Figure 2A,B

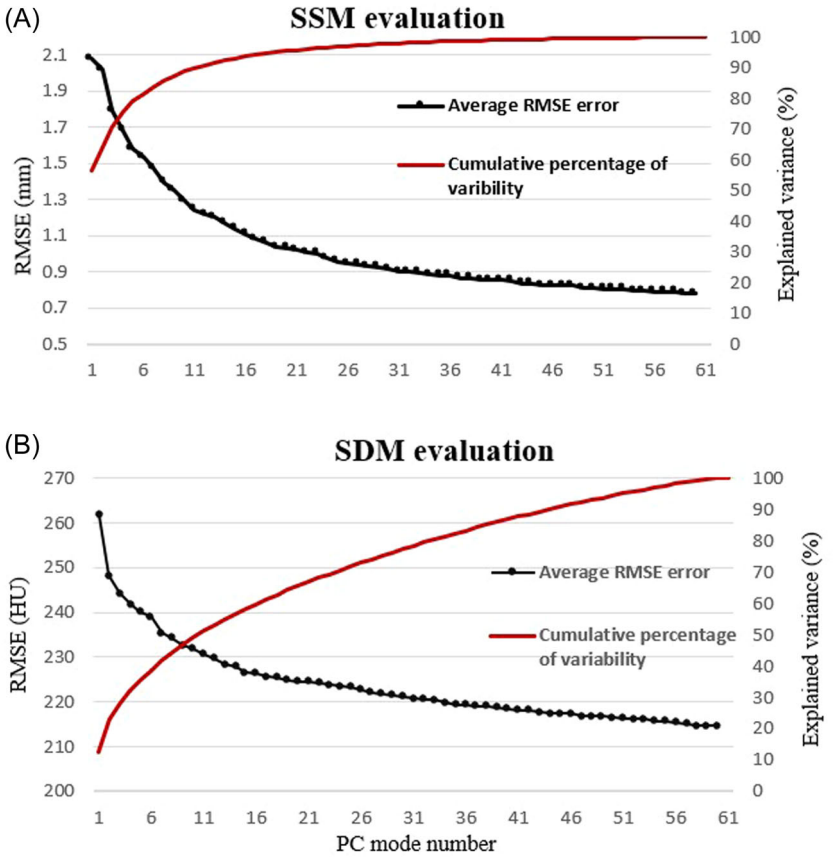

FIGURE 2 The cumulative percentage of variability, explained by adding each PC mode (red line) as well as the average root mean square generalization error (RMSE) (black line) for SSM (A) and SDM (B). PC, principal component; SDM, statistical density model; SSM, statistical shape model. [Color figure can be viewed at wileyonlinelibrary.com]

(black line), respectively. In the compact models, RMSE averaged 1.39 ± 0.28 mm (Figure 2A) and 227.12 ± 29.84 HU (Figure 2B), respectively. The overall range of HU for all subjects was −350 to 1677 HU.

3.2 | Scapular shape variations modes

The first four significant modes of shape variation, accounting for 75.6% of the variability, are represented by perturbing μ_S by $2SD_{SSM}$ (Supporting Information: Figure S–1 and Animations 1–4). The results related to clinical interpretation and anatomical measurements of SSM modes are provided in Supporting Information (Supporting Information: Tables S-1 and S-2).

The first mode, explaining 56.7% of the variability, mainly describes uniform scaling (Supporting Information: Animation 1 and Figure S-1) and significant correlations with increasing glenoid height and width, scapular offset, and fulcrum axis length (Supporting Information: Tables S-1 and S-2). *The second mode*, explaining 7.3% of the variability, primarily described the glenoid erosion size and coracoacromial complex rotation (Supporting Information: Animation 2, Figure S-1, and Tables S-1 and S-2). *The third mode*, explaining 6.8% of the variability, had the largest impact on glenoid orientation (version and inclination) in association with changes in PAS. *The fourth mode*, explaining 4.8% of the remaining variability, was mainly related to acromion orientation (posterior acromion–scapular plane angle and PAS). Subjects' gender significantly correlated with the first mode ($r = 0.75$ $p < 0.05$), whereas no correlation was found for age, BMI, or shoulder side with any of the modes.

3.3 | Bone density variations modes

The mean and first four main modes of BMDD variations are illustrated in two cross-sections of the mean scapular shape (Figure 3). The first one is a transverse cross-section through the glenoid center and TS and perpendicular to the scapular plane. The second one is located 2 mm underneath the glenoid surface and parallel to it (showing the subchondral bone). The mean BMDD shows higher bone density in the posterior–inferior region of the glenoid and less bone density in the central and anterior parts of the glenoid vault (Figure 3 and Supporting Information: Animation 5). BMDD variations were identified in all regions of the glenoid cavity (Figure 3).

The first mode of variation, explaining 12.7% of variability, primarily accounts for a slight increase of bone density at the posterior region of the glenoid vault and subchondral bone in association with decreasing bone density in the anterior and inferior regions (Figure 3). *The second mode*, explaining 10.4% of the variability, accounts for a uniform increase in density across the entire glenoid (Figure 3). *The third mode*, explaining 5.2% of the variability, primarily captures changes in density within the central and anterior part of the glenoid, varying from having high bone

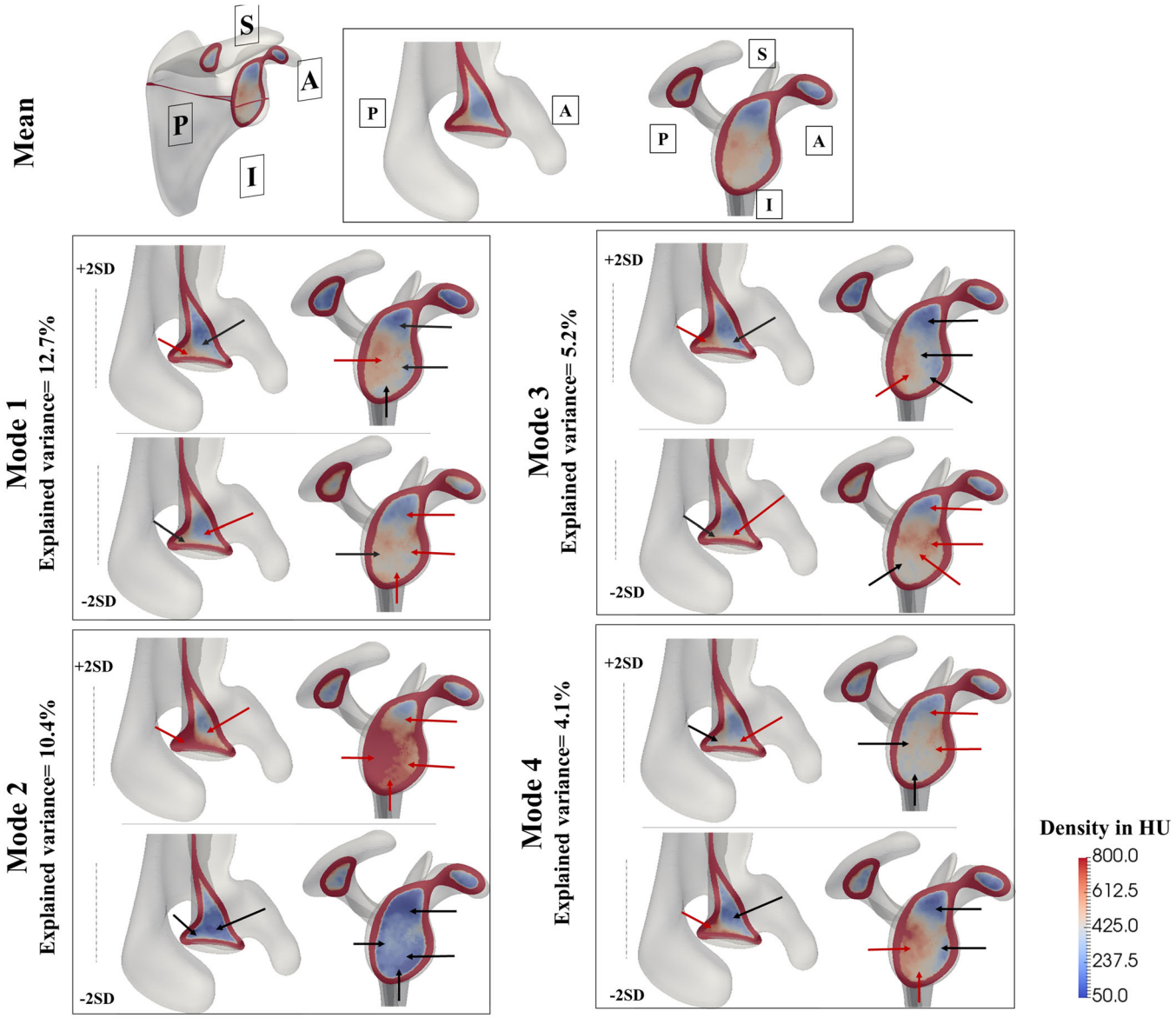

FIGURE 3 The colormaps illustrate the effects of perturbing the mean distribution of the bone mineral density (μ_I) by $2SD_{SDM}$ for each of the first four modes' variations, in two cross-sections of the mean shape of the scapula: The first transverse cross-section is defined perpendicular to the scapular plane, through the glenoid center and trigonum spinae, whereas the second plane is a plane defined 2 mm underneath, and parallel with the glenoid surface. Posterior (P), anterior (A), superior (S), and inferior (I) regions are indicated in the top box. Red arrows point to the primary observed regions with increased bone mineral density with respect to the mean, while black arrows point to the regions with decreased density associated with each of the individual principal component modes. [Color figure can be viewed at wileyonlinelibrary.com]

density localized in the center ($\mu_I - 2SD_{SDM}$) and a uniform distribution in the glenoid vault to an overall lower bone density with only the inferior-posterior part maintaining higher bone density ($\mu_I + 2SD_{SDM}$). *The fourth mode* (explaining 4.1% of the variability) represents a more pronounced reduction in density in the posterior and inferior regions as well as an increased density in the anterior-superior part of the glenoid vault and glenoid subchondral bone (Figure 3). BMI significantly correlated with the first mode only ($r = 0.34$ $p = 0.009$) and gender with the fourth mode only ($r = 0.33$ $p = 0.01$). No correlations were found for the subject's age or shoulder side.

3.4 | Covariation patterns between bone shape and density

By performing PLSC between significant PC scores of SSM and SDM, eight pairs of PLSC scores were identified. Based on the statistical significance test, four significant main modes of covariation, explaining 66% of the existing covariations were detected. The PLSC analysis revealed significantly strong correlation coefficients between scapular shape variations and BMDD in these four PLSC modes with correlation values of 0.89, 0.85, 0.70, and 0.62, all demonstrating *p*-values less than 0.001, affirming the strength of these relationships.

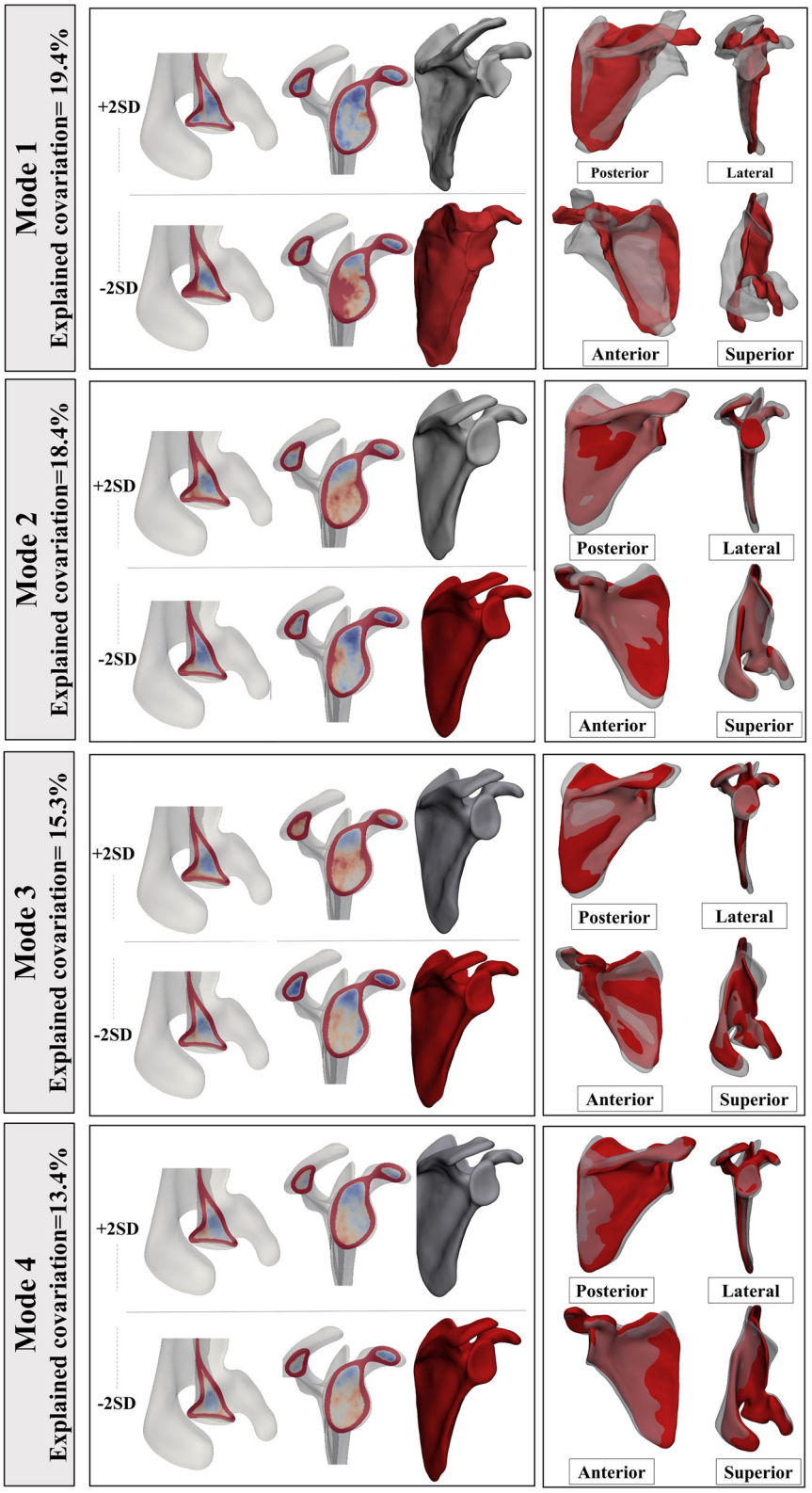

FIGURE 4 Visualization of the significant mode of scapular shape and bone mineral density distribution covariations (PLSC modes). For each mode, variations in scapular shape in four views (posterior, anterior, lateral, and anterior) are depicted. Red scapulae are showing the mean shape (μ_S) $-2SD_{PLSC}$ in each PLSC mode, while the white ones showing the mean shape (μ_S) $+2SD_{PLSC}$. Bone density distributions corresponding to each of the scapular shapes, mapped on the mean scapular shape, are also shown in the left-side boxes. PLSC, partial least square correlation. [Color figure can be viewed at wileyonlinelibrary.com]

Scapular shape variations associated with each PLSC mode and their respective covariations in BMDD are shown in Figure 4 and Supporting Information: Animations 6–9. The anatomical measurements related to these scapular covariations are summarized in Table 2.

The Pearson correlations of scapular PLSC scores with each subject's anatomical measurements are presented in Table 3. *The first mode* of covariation shows that increasing the scapular shape PLSC scores from $\mu_S - 2SD_{PLSC}$ (Figure 4, red scapula) to $\mu_S + 2SD_{PLSC}$ (Figure 4, gray scapula) is associated with a reduced postero–inferior

TABLE 2 Anatomical measurements corresponding to digitally generated scapulae by perturbing the mean shape by ±2SD of the PLSC scores.

		PLSC 1		PLSC 2		PLSC3		PLSC 4	
Anatomical measurements	**Mean (μ_S)**	**μ_S −2SD**	**μ_S +2SD**	**μ_S −2SD**	**μ_S +2SD**	**μ_S −2SD**	**μ_S +2SD**	**μ_S −2SD**	**μ_S +2SD**
Glenoid height (mm)	38.5	24.9	32.6	25.8	31.3	27.5	29.7	28.8	28.4
Glenoid width (mm)	29.4	41.0	40.7	33.9	42.8	37.7	38.7	38.2	38.2
Height-to-width ratio	1.3	1.7	1.3	1.3	1.4	1.4	1.3	1.3	1.4
Version angle (°)	15.7	26.3	2.1	6.7	18.8	17.9	9.2	−11.3	15.6
Inclination angle (°)	4.7	−14.7	22.8	10.5	2.1	3.7	7.7	1.5	9.9
CSA (°)	28.3	32.7	20.4	31.2	24.5	26.9	29.3	28.2	27.1
PAS (°)	67.0	59.8	68.3	67.0	66.3	64.2	68.6	65.5	67.4
LAA (°)	92.5	93.3	90.9	96.7	89.2	95.8	89.9	90.4	94.7
Scapula offset	100.6	92.2	110.4	102.5	100.2	99.0	103.6	101.9	101.0
Coracoid scapular plane angle (°)	59.3	41.9	70.9	60.9	58.0	61.1	58.8	61.6	57.9
Anterior acromion–scapular plane angle (°)	10.0	31.1	−13.8	8.3	9.9	16.1	−4.6	−7.8	11.8
Posterior acromion–scapular plane angle (°)	61.4	63.4	58.0	57.8	63.9	66.3	55.4	61.9	61.1
Fulcrum axis (mm)	70.8	63.5	79.3	66.1	77.5	74.6	69.0	67.8	75.4
Fulcrum axis ratio (%)	53.6	65.5	45.9	50.2	56.1	55.0	51.2	51.2	54.9

Abbreviations: CSA, critical shoulder angle; LAA, lateral acromial angle; PAS, posterior acromial slope; PLSC, partial least square correlation.

TABLE 3 Pearson correlation between subjects' scapular shape PLSC score of the first significant four modes and their anatomical measurements.

	Pearson correlation			
Anatomical measurements	**PLSC1**	**PLSC 2**	**PLSC 3**	**PLSC 4**
Glenoid height (mm)	−0.10	**0.66***	0.11	−0.04
Glenoid width (mm)	0.18	**0.52***	0.11	−0.08
Height-to-width ratio	−0.39	0.09	−0.02	0.06
Version angle (°)	−0.16	0.07	0.11	0.15
Inclination angle (°)	**0.58***	−0.18	0.05	0.24
CSA (°)	**−0.44***	−0.35	0.13	−0.08
PAS (°)	0.24	0.03	0.11	0.03
LAA (°)	−0.09	−0.29	−0.20	0.14
Scapula offset	0.21	0.24	0.19	−0.15
Coracoid scapular plane angle (°)	**0.49***	0.05	<0.001	−0.13
Anterior acromion–scapular plane angle (°)	**−0.53***	0.05	−0.18	0.37
Posterior acromion–scapular plane angle (°)	−0.17	0.15	−0.26	0.01
Fulcrum axis (mm)	0.21	**0.62***	−0.10	0.11
Fulcrum axis ratio (%)	**−0.41***	0.13	−0.23	0.20

Note: Bold values indicate correlations with $p < 0.0008$.

Abbreviations: CSA, critical shoulder angle; LAA, lateral acromial angle; PAS, posterior acromial slope; PLSC, partial least square correlation.

*Correlations with $p < 0.0008$.

erosion (significant increase of superior inclination and a trend for decreasing retroversion, and increasing scapular offset), a significant decrease of CSA and fulcrum axis ratio and a trend for increasing glenoid width to length ratio. This mode is furthermore associated with the anterior rotation of the coracoid, increasing acromion width size and anterior acromion–scapular plane angle (causing a less flat acromion in the sagittal plane). These changes in scapular shape covary with a reduction of bone density in the glenoid region in association with increasing bone density in the central and anterior parts of the glenoid vault (Figure 4 and Supporting Information: Animation 6). *The second mode* shows a significant increase in glenoid size and fulcrum axis length. In this mode, we can also see an increasing trend for CSA in association with decreasing superior inclination. All these variations in scapular shape covary with an increase in bone density all over the glenoid and its vault (Figure 4 and Supporting Information: Animation 7). *The third mode* represents increasing trends for the anterior and posterior angle of the acromion with the scapular plane, fulcrum axis ratio, decreasing CSA, and lateral shortening of the acromion roof to be associated with the presence of reducing bone density in the glenoid center (Figure 4 and Supporting Information: Animation 8). *The fourth mode* showed that decreasing anterior acromion–scapular plane angle and glenoid inclination covary with an increase in bone density in the anterior and central region of the glenoid (Figure 4 and Supporting Information: Animation 9). Patients' age moderately correlated with the first PLSC mode ($r = 0.33$, $p < 0.05$), and their gender was highly correlated with the second mode ($r = 0.6$, $p < 0.05$). No correlations were observed between biometric data and the two other PLSC modes.

4 | DISCUSSION

In this study, we developed accurate and independent SSM and SDM, which represented the scapular shape and bone density in B glenoids, respectively. Using the PLSC method, we revealed patterns of strong covariations between bone shape and density. The primary mode of covariation was between posterior–inferior glenoid erosion and posterior sclerotic bone formation in association with the reduction of bone density in the anterior and central regions of the glenoid.

To achieve the first goal, significant modes of variability were found for the SSM and SDM, representing 86% and 57% of their corresponding variability, respectively. The relatively high compactness of the SSM as well as the lower compactness of the SDMs are in agreement with the previous literature.[11,18,36] We evaluated the accuracy of the SSM and SDM in reconstructing the left-out subject by measuring RMSE, which were in line with previous studies, albeit they were typically performed on an assumed less-challenging population of healthy scapula.[11,18,22,36]

Our SSM-based first variation mode confirms uniform scapula scaling observed in prior studies.[11,18,22,36] However, the second and third modes showed variabilities that appear to be specifically associated with B glenoid pathologies. In these two SSM modes, increasing the size of posterior–inferior glenoid erosion in association with posterior rotation of the coracoacromial complex (the second mode) and variability in the orientation of the glenoid (increasing glenoid inferior inclination and decrease of glenoid retroversion) in association with a steeper acromion slope (the third mode) were identified. Although SSM method has been used for describing variations in healthy scapulae, predicting premorbid glenoid cavity, and also quantification of glenoid bone defects,[37–40] to our knowledge, describing variation in eroded scapular morphology is only limited to one study focusing on B glenoids.[19] While they did observe some variations similar to those in our study, the erosion-related SSM mode of our research (specifically, posterior inferior erosion as our second mode of variation) was exclusively identified as inferior erosion variation in their study. This can be attributed to the fact that their study specifically concentrated on B2 and B3 glenoids, both of which are known for their common occurrence of posterior erosion. Consequently, the lack of variability in this regard was expected. Furthermore, studies conducted on healthy population have identified variations in the rotation of the coracoacromial complex, acromion slope, and coracoid orientation similar to our study.[32] These variations could impact glenohumeral mechanics by affecting the distribution of deltoid muscle force and the direction of supraspinatus muscle action.[32] By utilizing B glenoid SSM, we captured the association of these variabilities with variations in size of glenoid erosions and glenoid orientation. However, the temporal sequence of pathologic changes and their causality are unknown and need further investigation.

In our SDM, in contrast with healthy glenoids where the center of the glenoid typically has the best bone quality,[11] B glenoid showed higher average bone density in the posterior–inferior. This aligns with previous studies indicating that the posterior bony quadrants of the glenoid are typically denser than the anterior quadrants in patients with asymmetric glenoid erosion (especially B glenoids).[15–17] The first and fourth SDM modes of variations, identified significant variability in BMDD in the posterior and inferior regions as well as high variability in the bone density of the anterior glenoid vault, while the second mode accounts for overall changes in the entire bone quality. The correlation between these first and fourth SDM modes and patients' BMI and gender showed that females and patients with higher BMI have more asymmetrical BMDD. Bone density variability in the posterior and inferior part of the glenoid was observed in the previous study of B glenoids (B2 and B3), however, it is important to note that not all modes corresponded to each other as we examined more localized regions and a broader group of B glenoids, including B1, B2, and B3 subtypes.[36] Identification of these asymmetrical BMDD and the following asymmetrical distribution of bone stress after glenoid component implantation[14] can be considered as one of the possible reasons behind glenoid component loosening in B glenoids.

For the second objective, we used the PLSC method to explore the scapular morphology and BMDD covariation patterns. Previous studies assessed the Pearson correlation between SSM and SDM PC scores to investigate the association between scapular shape and BMDD.[11,18] These studies did not find strong correlations between BMDD and shape variations.[11,18] Our PLSC method instead, by maximizing covariation between two data sets, allowed quantifying scapular morphology variations patterns that have the strongest covariation with specific BMDD variation patterns. Using this method, the main mode of covariation identified posterior–inferior erosion and joint line medialization to correspond with increased density of the posterior glenoid region and a loss of bone density in the central and anterior part of the glenoid vault. This covariation seems to correspond with alterations in joint loading and associated bone remodeling according to Wolff's law.[41] Posterior glenoid erosion is associated with posterior humeral head migration,[42] which may induce higher mechanical loading to the inferior-posterior region, leading to the denser bone in these regions, and unloading the central and anterior parts. In this main mode, we observed variations in acromion shape and increasing fulcrum axis ratio, which were reported to be associated with a more asymmetric distribution of the deltoid muscle force, as well as changes in the supraspinatus muscle line of action.[32] This information may provide us with more evidence for the possible alternations in force distributions and the following bone density adaptations. The second covariation mode and, more specifically, its association with biometric data, suggests that female B glenoid patients with a smaller glenoid, increased retroversion, and inferior inclination present severely reduced bone density in the entire glenoid. Therefore, this group of patients needs further consideration during surgical planning. These findings highlight the potential of PLSC modes and the generated integrated scapular shape and density models as an integrated input for population-based finite element models for designing population-specific glenoid components and patient-specific planning.

This study suffers from some limitations. The first limitation pertains to the size and distribution of B glenoid subtypes. While the training set of 62 subjects was in the range of previous scapula studies (53–75 subjects[11,18,36]), it may not be fully representative of the entire population. Nonetheless, we are of the opinion that expanding the study population improves the chances of identifying new variations and covariation patterns without limiting the patterns already found in this study. Second, surface nodal registration was not possible for severely eroded glenoids (2 out of 64 subjects). Improving the registration algorithm could likely expand our training data set with more extreme cases. Third, 2 mm of the outer border of the bone was excluded in the SDM development to account for possible surface artifacts. However, we believe this has no major impact on the conclusions of this study, as this 2 mm corresponds to the minimal amount of reaming that is classically performed before glenoid component implantation to accommodate the glenoid implant backside.[43] Furthermore, bone quality and risk of bone failure can be influenced by factors other than BMD, which was the only focus of this study. Additional factors, such as bone volume fraction, architectural characteristics, the presence of microdamage, and so on.[44–46] However, previous literature emphasized on significant correlation between reduced BMD and an elevated risk of glenoid component fixation failure.[12–14] Consequently, the findings of our study hold considerable importance in the context of glenoid component fixation and failure. Finally, the low compactness of the resulting SDM, already observed in previous studies, can be related to the high 3D BMDD variability across specimens different imaging protocols, the lack of a calibration phantom, or difficulties related to the interior elements registrations in the volumetric mesh morphing due to the absence of unique features to drive the mesh morphing.[18,36] However, the developed SDM has a comparable compactness with other studies and effectively identifies the main pattern of variations.

In conclusion, this research established the use of SSM, SDM, and the PLSC methodology, confirming and identifying the significant covariations between BMDD and the scapular shape of B glenoids. The found covariation patterns, as well as a detailed description of bone shape and BMDD variations, can be used for generating more realistic synthetic models. The clinical relevance of this study lies in its ability to enhance patient-specific implant design and personalized surgical approaches by considering the compromise between the amount of glenoid bone correction and the quality of bone support, which is one of the main challenges during B glenoid surgeries.

AUTHOR CONTRIBUTIONS

Nazanin Daneshvarhashjin contributed to the image segmentation, development of the modeling approach, data analysis, interpretation of data, manuscript drafting, and writing. Philippe Debeer and Bernardo Innocenti contributed to the supervising the study and revising the manuscript. Filip Verhaegen and Lennart Scheys supervised the research and contributed to the research design, development of the modeling approach, interpretation of data, and revising the manuscript. All authors have read and approved the final submitted manuscript. No benefits in any form have been received or will be received from a commercial party related directly or indirectly to the subject of this article.

ACKNOWLEDGMENTS

The authors acknowledge the financial support from Zimmer Biomet (EDW-ZIMMER-O2030) and the PROSPEROS project (ZL3C150100-401), funded by the Interreg VA Flanders–The Netherlands program. No benefits in any form have been received or will be received from a commercial party related directly or indirectly to the subject of this article.

ORCID

Nazanin Daneshvarhashjin http://orcid.org/0000-0002-3856-1167
Bernardo Innocenti http://orcid.org/0000-0001-8992-8865
Filip Verhaegen http://orcid.org/0000-0003-0469-6052
Lennart Scheys http://orcid.org/0000-0002-1727-533X

REFERENCES

1. Castagna A, Garofalo R. Journey of the glenoid in anatomic total shoulder replacement. *Shoulder Elbow*. 2019;11(2):140-148.
2. Scarcella MJ, Yalcin S, Ginesin E, Patel R, Miniaci A. Treatment options for complex shoulder osteoarthritis with posterior humeral head subluxation and glenoid bone loss (Walch B): a systematic review. *JSES Rev Rep Tech*. 2022;2(3):285-296. https://www.sciencedirect.com/science/article/pii/S266663912200058X
3. Bohsali KI, Bois AJ, Wirth MA. Complications of shoulder arthroplasty. *J Bone Jt Surg*. 2017;99(3):256-269.
4. Gonzalez JF, Alami GB, Baque F, Walch G, Boileau P. Complications of unconstrained shoulder prostheses. *J Shoulder Elbow Surg*. 2011;20(4):666-682.
5. McLendon PB, Schoch BS, Sperling JW, Sánchez-Sotelo J, Schleck CD, Cofield RH. Survival of the pegged glenoid component in shoulder arthroplasty: part II. *J Shoulder Elbow Surg*. 2017;26(8):1469-1476.
6. Papadonikolakis A, Neradilek MB, Matsen FA. Failure of the glenoid component in anatomic total shoulder arthroplasty. *J Bone Jt Surg*. 2013;95(24):2205-2212.
7. Grantham WJ, Dekker TJ, Lacheta L, et al. Total shoulder arthroplasty outcomes after noncorrective, concentric reaming of B2 glenoids. *JSES Int*. 2020;4(3):644-648.
8. Roche CP, Diep P, Grey SG, Flurin P-H. Biomechanical impact of posterior glenoid wear on anatomic total shoulder arthroplasty. *Bull NYU Hosp Jt Dis*. 2013;71(2):S5.
9. Ho JC, Amini MH, Entezari V, et al. Clinical and radiographic outcomes of a posteriorly augmented glenoid component in anatomic total shoulder arthroplasty for primary osteoarthritis with posterior glenoid bone loss. *J Bone Jt Surg*. 2018;100(22):1934-1948.
10. Yongpravat C, Kim HM, Gardner TR, Bigliani LU, Levine WN, Ahmad CS. Glenoid implant orientation and cement failure in total shoulder arthroplasty: a finite element analysis. *J Shoulder Elbow Surg*. 2013;22(7):940-947.
11. Burton WS, Sintini I, Chavarria JM, Brownhill JR, Laz PJ. Assessment of scapular morphology and bone quality with statistical models. *Comput Methods Biomech Biomed Engin*. 2019;22(4):341-351.
12. Chamseddine M, Breden S, Pietschmann MF, Müller PE, Chevalier Y. Periprosthetic bone quality affects the fixation of anatomic glenoids

in total shoulder arthroplasty: in vitro study. *J Shoulder Elbow Surg*. 2019;28(1):e18-e28.
13. Terrier A, Obrist R, Becce F, Farron A. Cement stress predictions after anatomic total shoulder arthroplasty are correlated with preoperative glenoid bone quality. *J Shoulder Elbow Surg*. 2017; 26(9):1644-1652.
14. Chevalier Y, Santos I, Müller PE, Pietschmann MF. Bone density and anisotropy affect periprosthetic cement and bone stresses after anatomical glenoid replacement: a micro finite element analysis. *J Biomech*. 2016;49(9):1724-1733.
15. Knowles NK, Athwal GS, Keener JD, Ferreira LM. Regional bone density variations in osteoarthritic glenoids: a comparison of symmetric to asymmetric (type B2) erosion patterns. *J Shoulder Elbow Surg*. 2015;24(3):425-432.
16. Letissier H, Chaoui J, Bercik MJ, et al. Glenoid subchondral bone density in osteoarthritis: a comparative study of asymmetric and symmetric erosion patterns. *Orthop Traumatol Surg Res*. 2020;106(6): 1127-1134. https://www.sciencedirect.com/science/article/pii/S1877705682030195X
17. Chen X, Reddy AS, Kontaxis A, et al. Version correction via eccentric reaming compromises remaining bone quality in B2 glenoids: a computational study. *Clin Orthop Relat Res*. 2017;475 (12):3090-3099.
18. Soltanmohammadi P, Elwell J, Veeraraghavan V, Athwal GS, Willing R. Investigating the effects of demographics on shoulder morphology and density using statistical shape and density modeling. *J Biomech Eng*. 2020;142(12):121005.
19. Sharif-Ahmadian A, Beagley A, Pearce C, Saliken D, Athwal GS, Giles JW. Statistical shape and bone property models of clinical populations as the foundation for biomechanical surgical planning: application to shoulder arthroplasty. *J Biomech Eng*. 2023;145:101004.
20. Manthey L, Ousley SD. Chapter 5.3—Geometric morphometrics. In: Obertová Z, Stewart A, Cattaneo C, eds. *Statistics and Probability in Forensic Anthropology*. Academic Press; 2020:289-298. https://www.sciencedirect.com/science/article/pii/B978012815764000023X
21. Abdi H, Williams LJ. Partial least squares methods: partial least squares correlation and partial least square regression. In: Reisfeld B, Mayeno AN, eds. *Computational Toxicology*. Vol II. Humana Press; 2013:549-579. doi:10.1007/978-1-62703-059-5_23
22. Verhaegen F, Meynen M, Debeer P, Scheys L. Determination of predisposing scapular anatomy with a statistical shape model–part II: shoulder osteoarthritis. *J Shoulder Elb Surg*. 2021;30:e558-e571.
23. Bercik MJ, Kruse II, K, Yalizis M, Gauci MO, Chaoui J, Walch G. A modification to the Walch classification of the glenoid in primary glenohumeral osteoarthritis using three-dimensional imaging. *J Shoulder Elbow Surg*. 2016;25(10):1601-1606.
24. Verhaegen F, Meynen A, Matthews H, Claes P, Debeer P, Scheys L. Determination of pre-arthropathy scapular anatomy with a statistical shape model: part I—rotator cuff tear arthropathy. *J Shoulder Elbow Surg*. 2020;30:1095-1106.
25. White JD, Ortega-Castrillón A, Matthews H, et al. MeshMonk: open-source large-scale intensive 3D phenotyping. *Sci Rep*. 2019;9(1):6085.
26. Stegmann MB, Gomez DD. A brief introduction to statistical shape analysis. Informatics and Mathematical Modelling, Technical University of Denmark, DTU 15(11). 2002.
27. Grassi L, Väänänen SP, Isaksson H. Statistical shape and appearance models: development towards improved osteoporosis care. *Curr Osteoporos Rep*. 2021;19:676-687.
28. Vasco M. Permutation tests to estimate significances on principal components analysis. *Comput Ecol Softw*. 2012;2(2):103.
29. Abdi H. Partial least squares regression and projection on latent structure regression (PLS regression). *WIREs Comput Stat*. 2010;2(1):97-106.
30. Young NM, Sherathiya K, Gutierrez L, et al. Facial surface morphology predicts variation in internal skeletal shape. *Am J Orthod Dentofacial Orthop*. 2016;149(4):501-508.
31. Abdi H, Williams LJ. Partial least squares methods: partial least squares correlation and partial least square regression. In: Reisfeld B, Mayeno A, eds. *Computational Toxicology*. Springer; 2013:549-579.
32. Casier SJ, Van den Broecke R, Van Houcke J, Audenaert E, De Wilde LF, Van Tongel A. Morphologic variations of the scapula in 3-dimensions: a statistical shape model approach. *J Shoulder Elbow Surg*. 2018;27(12):2224-2231.
33. Jacquot A, Gauci M-O, Urvoy M, de Casson FB, Berhouet J, Letissier H. Anatomical plane and transverse axis of the scapula: reliability of manual positioning of the anatomical landmarks. *Shoulder Elb*. 2021;14:491-499.
34. Terrier A, Ston J, Larrea X, Farron A. Measurements of three-dimensional glenoid erosion when planning the prosthetic replacement of osteoarthritic shoulders. *Bone Joint J*. 2014;96(4):513-518.
35. Bland JM, Altman DG. Statistics notes: multiple significance tests: the Bonferroni method. *BMJ*. 1995;310(6973):170.
36. Sharif Ahmadian A. Development of statistical shape and intensity models of eroded scapulae to improve shoulder arthroplasty. 2021. https://dspace.library.uvic.ca/handle/1828/13635
37. Plessers K, Vanden Berghe P, Van Dijck C, et al. Virtual reconstruction of glenoid bone defects using a statistical shape model. *J Shoulder Elbow Surg*. 2018;27(1):160-166.
38. Plessers K, Verhaegen F, Van Dijck C, et al. Automated quantification of glenoid bone defects using 3-dimensional measurements. *J Shoulder Elbow Surg*. 2020;29:1050-1058.
39. Abler D, Berger S, Terrier A, Becce F, Farron A, Büchler P. A statistical shape model to predict the premorbid glenoid cavity. *J Shoulder Elbow Surg*. 2018;27(10):1800-1808.
40. Salhi A, Burdin V, Boutillon A, Brochard S, Mutsvangwa T, Borotikar B. Statistical shape modeling approach to predict missing scapular bone. *Ann Biomed Eng*. 2020;48(1):367-379.
41. Wolff J. Das gesetz der transformation der knochen, Berlin, a. hirchwild. Law Bone Remodel. 1892.
42. Verhaegen F, Meynen A, Pitocchi J, Debeer P, Scheys L. Quantitative statistical shape model-based analysis of humeral head migration, part 2: shoulder osteoarthritis. *J Orthop Res*. 2023;41(1):21-31.
43. Yongpravat C, Lester JD, Saifi C, et al. Glenoid morphology after reaming in computer-simulated total shoulder arthroplasty. *J Shoulder Elbow Surg*. 2013;22(1):122-128. https://www.sciencedirect.com/science/article/pii/S1058274612000237
44. Wallace JM. Chapter 7—Skeletal hard tissue biomechanics. In: Burr DB, Allen MR, eds. *Basic and Applied Bone Biology*. 2nd ed. Academic Press; 2019:125-140. https://www.sciencedirect.com/science/article/pii/B9780128132593000075
45. Follet H, Boivin G, Rumelhart C, Meunier PJ. The degree of mineralization is a determinant of bone strength: a study on human calcanei. *Bone*. 2004;34(5):783-789. https://www.sciencedirect.com/science/article/pii/S8756328203004733
46. Burr DB. Bone morphology and organization. In: Burr DB, Allen MR, eds. *Basic and Applied Bone Biology*. Elsevier; 2019:3-26.

SUPPORTING INFORMATION

Additional supporting information can be found online in the Supporting Information section at the end of this article.

How to cite this article: Daneshvarhashjin N, Debeer P, Innocenti B, Verhaegen F, Scheys L. Covariations between scapular shape and bone density in B-glenoids: a statistical shape and density modeling-approach. *J Orthop Res*. 2023; 1-11. doi:10.1002/jor.25747